ACS OMEGA

Article

Cite This: ACS Omega 2018, 3, 5012−5020

Ultrasonic-Assisted Preparation, Characterization, and Use of Novel Biocompatible Core/Shell Fe_3O_4@GA@Isinglass in the Synthesis of 1,4-Dihydropyridine and 4*H*-Pyran Derivatives

Elham Pourian,[†] Shahrzad Javanshir,*[,†] Zahra Dolatkhah,[†] Shiva Molaei,[†] and Ali Maleki[‡]

[†]Heterocyclic Chemistry Research Laboratory, Department of Chemistry, and [‡]Catalysts and Organic Synthesis Research Laboratory, Department of Chemistry, Iran University of Science and Technology, Tehran 16846-13114, Iran

Supporting Information

ABSTRACT: This work focussed on the synthesis of a new catalytic material isinglass (IG)-based Fe_3O_4@GA@IG core/shell magnetic nanoparticles and the investigation of its catalytic activity in two important multicomponent reactions. Fe_3O_4 nanoparticles were prepared using a simple coprecipitation method and then coated with IG consisting predominantly of the protein collagen in the presence of glutaraldehyde as a cross-linking agent. The obtained hybrid material has been characterized by Fourier transform infrared analysis, scanning electron microscopy, transmission electron microscopy (TEM), vibrating sample magnetometry, energy-dispersive X-ray, X-ray diffraction (XRD), and Brunauer−Emmett−Teller analyses. The results of XRD analysis implied that the prepared nanocomposite consists of two compounds of crystalline magnetite and amorphous IG, and the formation of its core/shell structure had been confirmed by TEM images. The catalytic performance of the as-prepared core/shell bionanocatalyst was evaluated for the first time in the synthesis of 1,4-dihydropyridine and 4*H*-pyran derivatives under sonication in ethanol. This core/shell structure because of the superparamagnetic property of Fe_3O_4 and unique properties of IG as a bifunctional biocatalyst offers a high potential for many catalytic applications. Recycling study revealed that no significant decrease in the catalytic activity was observed even after six runs.

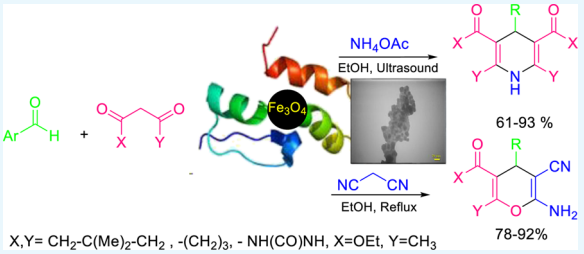

1. INTRODUCTION

In recent years, sonochemistry as one of the greenest and effective techniques has been considered in the synthesis of various bulk and nanomaterials. The synthesis of substances by ultrasonic irradiation requires less amounts of solvents and catalysts, which better meets the ecological requirements. In the liquid medium, cavitation is the predominant phenomenon induced by ultrasound. The phenomenon of acoustic cavitation corresponds to the creation, growth, and then implosion (collapse) of bubbles formed when a liquid is subjected to a periodic pressure wave. The implosion of the bubble then locally causes the release of a large amount of thermal energy (locally, the temperature can reach 5000 °C and the pressure of several hundred atmospheres) and mechanical energy (jet emission of liquids moving at a speed of 100 meters per second) without any significant change in the whole medium (in terms of temperature and pressure).[1,2] Because of its unusual properties, this technique has been extensively used.

The development of new hybrid materials combining organic and inorganic compounds to improve their properties for catalytic applications is a challenge that has always existed. In the field of the development of adaptive materials, hybrid materials with a polymer component make it possible to answer a large number of environmental or societal problems via biomimetic approaches. Nature has always combined organic and inorganic components, at the nanoscale, to construct smart materials with remarkable properties and functions (mechanics, density, permeability, color, hydrophobicity, etc.). Shellfish carapaces, mollusk shells, bones, and tissues are examples of organic−inorganic natural materials.[3−5]

The field of functional materials is in constant search of materials with innovative properties. Depending on the functions involved, it is advantageous to combine properties of the material, normally present in different materials. One of the ways of increasing the number of interesting properties that a nanoparticle (NP) possesses is through the formation of particles with a core/shell structure.[3] Such a structure often makes it possible to combine the properties of two very different types of particles. Magnetic core/shell NPs have a huge potential for application because of the range of properties that can be envisaged for this type of materials.[4,5] Magnetically separable NPs can be functionalized with catalysts, working then at the boundary between homogeneous and heterogeneous catalysts, both being "in the solution" and separable by the application of an external magnetic field, resulting in remarkable catalyst recovery without the need for a filtration step.[6]

Received: March 2, 2018
Accepted: April 24, 2018
Published: May 8, 2018

DOI: 10.1021/acsomega.8b00379
ACS Omega 2018, 3, 5012−5020

Scheme 1. Preparation of the Fe_3O_4@GA@IG Bionanocatalyst

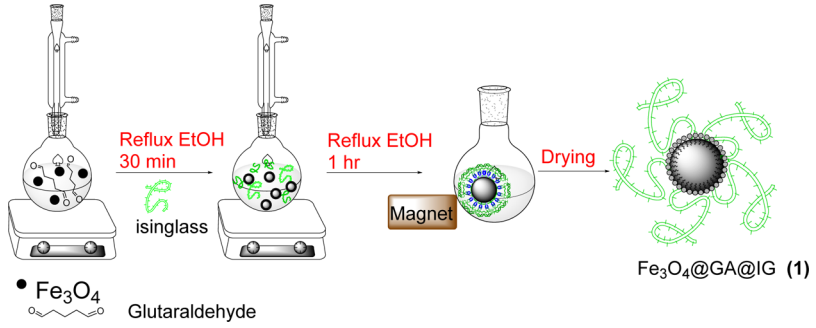

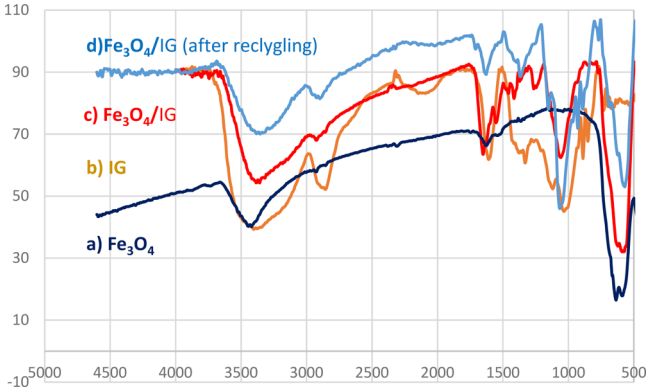

Figure 1. FT-IR spectra of (a) Fe_3O_4, (b) IG, (c) Fe_3O_4@GA@IG, and (d) Fe_3O_4@GA@IG after recycling.

Isinglass (IG) was derived from the swim bladders of certain tropical fish and consists predominantly of the protein collagen, which is readily soluble in organic acids. IG collagen exists as a rodlike triple helical molecule and is thermally labile.[7] IG consists of 90 basic side chain groups and 118 acid groups per thousand total residues. Because 41 of the acidic groups are in the amide form, there is an excess of basic groups and the protein; therefore, it has a basic character, that is, has a basic isoionic pH.[8] The total hydroxyl content of IG is high and in consequence has high hydrogen bonding capacity; thus, it is capable of bonding with many groups, such as C=O, OH, and so forth, on other compounds. Therefore, in continuation of our works using bionanocatalysts in organic synthesis,[9,10] we planned to functionalize Fe_3O_4 magnetic NPs (MNPs) with IG to prepare a bionanocatalyst for use in organic synthesis.

1,4-Dihydropyridine (1,4-DHP) and 4*H*-pyran structural architectures occur in many bioactive natural products and synthetic drugs, and these structural units serve as important chemical intermediates.[11−13] Consequently, several methods have been reported to promote their preparation.[14−40] Although most of these processes offer distinct advantages, some of them suffer from a few limitations such as prolonged and tedious catalyst preparation, using expensive and hazardous reagents and solvents, besides more catalyst loading.[38] Therefore, to overcome these disadvantages, a great deal of efforts is directed to develop a novel biocompatible catalytic system for the synthesis of these compounds. As a result, the present core/shell Fe_3O_4@GA@IG as a bionanocatalyst has been prepared (Scheme 1) and has been studied for the first time in the synthesis of 1,4-DHP and 4*H*-pyran derivatives via the one-pot multicomponent condensation of an aldehyde, a 1,3-dicarbonyl compound, and ammonium acetate under sonication condition in ethanol.

2. RESULTS AND DISCUSSION

2.1. Characterization of Fe_3O_4@GA@IG. The prepared magnetic nanocomposite Fe_3O_4@GA@IG structure was elucidated by Fourier transform infrared (FT-IR) analysis, scanning electron microscopy (SEM), transmission electron microscopy (TEM), vibrating sample magnetometry (VSM) analysis, thermogravimetric analysis (TGA), X-ray diffraction (XRD), Brunauer−Emmett−Teller (BET) technique, and energy-dispersive X-ray spectroscopy (EDX).

On the basis of the FT-IR spectra of Fe_3O_4@GA@IG, the presence of IG and Fe_3O_4 can be clearly observed by the characteristic absorption peaks present at 550 cm^{-1} related to Fe−O vibration (Figure 1c). Because of the fact that IG has a collagen structure, the main absorption bands were 3444−3100, 2900−2893, 1649, 1369, 1155, and 1074 cm^{-1}. The absorptions bands at 1369 and 1155 cm^{-1} might be accredited to the ν(C−N) and δ(N−H) absorptions of amide II, respectively. Amide I band associated with ν(C=O) absorptions could be found at 1649 cm^{-1}, the peaks at 2900−2893 cm^{-1} were attributed to $\nu(CH_2)$ and $\nu(CH_3)$ of amide B, and the band between 3444 and 3110 cm^{-1} corresponds to N−H stretching of amide A. Peak shifts of amide in Fe_3O_4@GA@IG were clearly observed (1649 in IG to 1651 cm^{-1} in Fe_3O_4@GA@IG). The observed

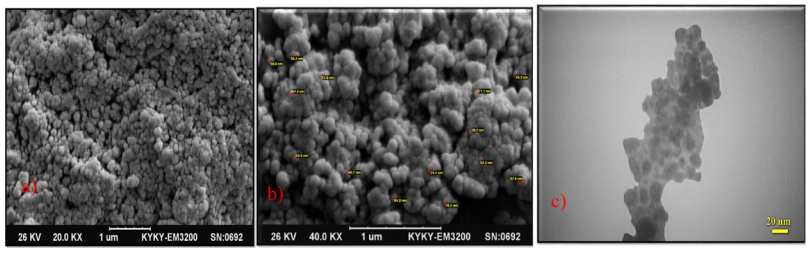

Figure 2. (a,b) SEM and (c) TEM images of the as-prepared Fe_3O_4@GA@IG core/shell nanocomposite.

DOI: 10.1021/acsomega.8b00379
ACS Omega 2018, 3, 5012−5020

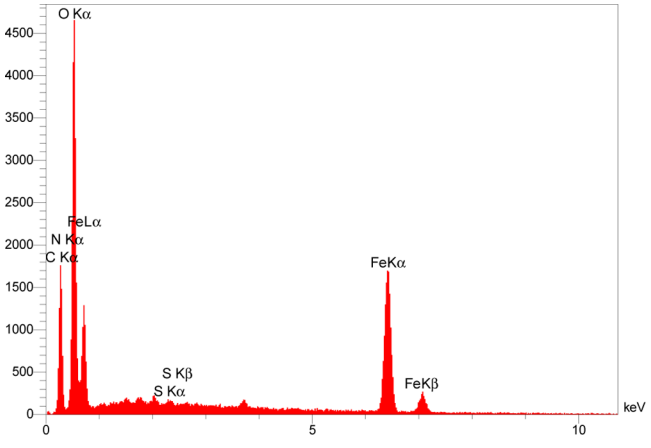

Figure 3. EDX analysis of Fe_3O_4@GA@IG.

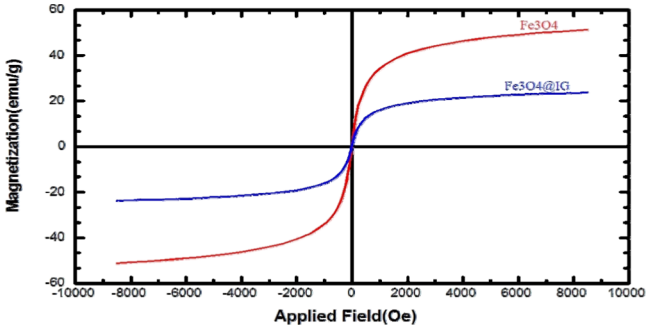

Figure 4. VSM analysis of Fe_3O_4@GA@IG.

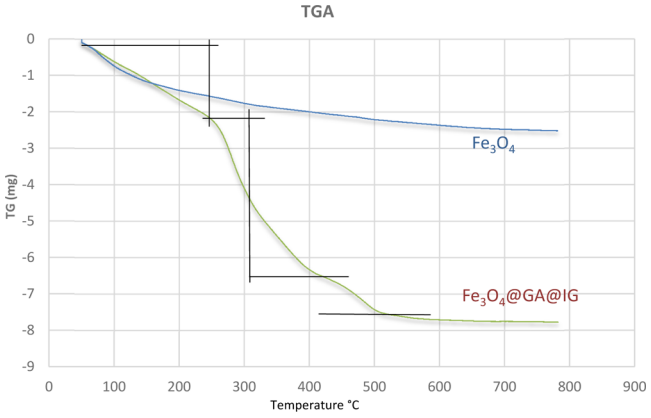

Figure 5. TGA analysis of Fe_3O_4@GA@IG.

shift in the infrared spectra is related to the chemical interaction between Fe_3O_4@GA NPs and IG.

As can be seen from the SEM analysis shown in Figure 2b, the average particle size was 63 nm. These images show a homogeneous and monotonous surface of the bionanocatalyst. Moreover, to verify the core/shell nanostructure of the as-prepared bionanocatalyst, its TEM images were provided. As shown in Figure 2c, the black centers represent the Fe_3O_4 core and the brightest areas show the IG shell.

The EDX analysis revealed that Fe, O, C, S, and N are the main elements present in the bionanocomposite with Fe being the most abundant (Figure 3).

The hysteresis loops of Fe_3O_4 MNPs and Fe_3O_4@GA@IG are exposed in Figure 4. As shown in the figure, the magnetization decreases from plateau state to zero on removal of the magnetic field for both NPs; neither coercivity (Hc) nor remanent magnetization (Mr) was observed in the hysteresis curves, which clearly indicates their superparamagnetic nature. The coverage of the surface of Fe_3O_4 NPs by IG is the origin of the reduction in saturation magnetization.

Table 1. Effect of the Catalyst, Catalyst Loading, Synthesis Condition, and Solvent on the Model Reaction

entry	cat. & cat. amount (mg)	solvent	temp. (°C)	time (min)	yield (%)
1			rt	120	trace
2			80	120	trace
3		ethanol	rt	120	trace
4		ethanol	reflux	120	25
5		ethanol	ultrasound	60	28
6	Fe_3O_4@IG (5)	ethanol	rt	120	32
7	Fe_3O_4@IG (5)	ethanol	50	120	45
8	Fe_3O_4@IG (5)	ethanol	reflux	90	77
9	Fe_3O_4@IG (5)	ethanol	ultrasound	30	91
10	Fe_3O_4@IG (5)	H_2O	rt	240	trace
11	Fe_3O_4@IG (5)	H_2O	reflux	180	trace
12	Fe_3O_4@IG (5)	H_2O	ultrasound	70	trace
13	Fe_3O_4@IG (5)	acetonitrile	reflux	120	56
14	Fe_3O_4@IG (5)	chloroform	reflux	120	51
15	Fe_3O_4@IG (10)	ethanol	ultrasound	20	94
16	Fe_3O_4@IG (15)	ethanol	ultrasound	15	92
17	Fe_3O_4 NPs (10)	ethanol	ultrasound	60	41
18	IG (10)	ethanol	ultrasound	60	78

TGA was carried out under inert nitrogen gas at a steady speed of 10 °C/min and 800 °C temperature.

As shown in the curve of Figure 5, the first mass loss of the magnetic bionanocatalyst occurred below 240 °C, which can be attributed to water thermodesorption from the surface (drying), whereas the second weight loss above 240 °C is associated with the release of hydroxyl ions from the NPs and volatilization. The third mass loss occurred at 411 °C and is due to the combustion of all carbon content.

According to the results of BET analysis, the specific surface area of the bionanocatalyst was 28.15 m^2/g. The volume of the single-point adsorption cavity is 0.142816 cm^3/g, and the single-point cavity dissipation volume is 0.159 cm^3/g. The particle size is 20 nm. Figure 6 shows the nitrogen absorption and depletion diagram of magnetic Fe_3O_4@GA@IG. The specific surface area of the IG catalyst is 1.20 m^2/g, and the cavity volume of the single point is 0.0024 cm^3/g. Also, Figure 6 shows the absorption and desorption diagram of nitrogen of IG. Because of the presence of Fe_3O_4 NPs, the catalyst has a significant increase in the specific surface area.

The XRD pattern of the magnetic nanocatalyst has been illustrated in Figure 7. In the XRD pattern of Fe_3O_4@GA@IG, on the basis of JCPDS card#19-629, the positions of diffraction peaks at 2θ = 30°, 35°,43°, 53°, 57°, 62°, and 74° were attributed to (220), (311), (400), (422), (511), (440), and (533) of Fe_3O_4 NPs, which was surrounded by the IG shell. Forasmuch as the main peaks of Fe_3O_4@GA@IG are the same as those of pure Fe_3O_4 NPs, which means that the crystal structure of Fe_3O_4 NPs is well-maintained even after the procedure of making a new MNP catalyst. Wide peaks of diffraction angles 10−23 are related to the amorphous property of IG on the surface of Fe_3O_4 NPs.

DOI: 10.1021/acsomega.8b00379
ACS Omega 2018, 3, 5012−5020

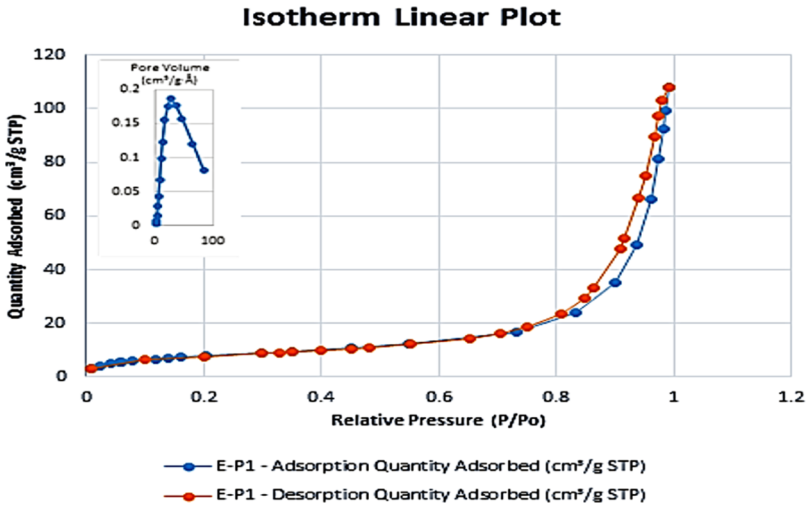

Figure 6. BET analysis of Fe_3O_4@GA@IG.

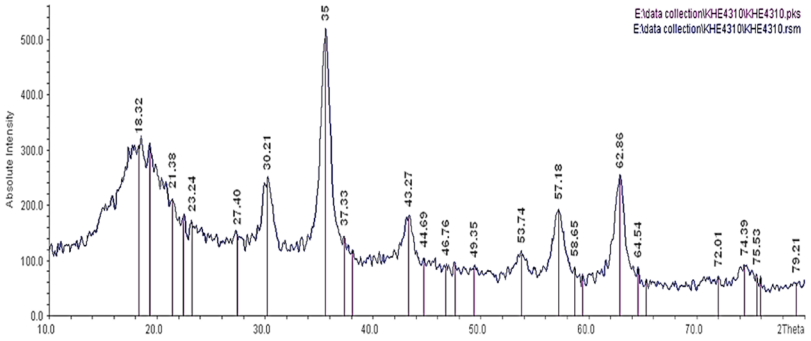

Figure 7. XRD analysis of Fe_3O_4@GA@IG.

Scheme 2. Plausible Mechanism of the Model Reaction for the 1,4-DHP and Polyhydroquinoline Derivative Synthesis

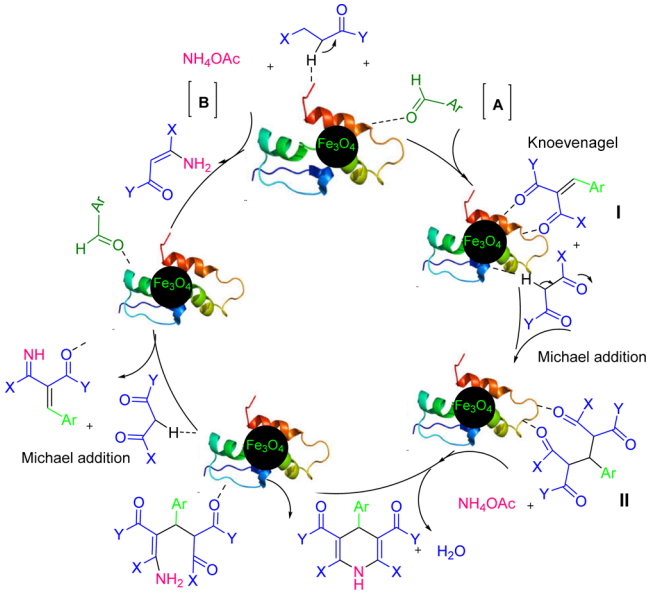

2.2. Synthesis of 1,4-DHP and Polyhydroquinoline Derivatives by Fe_3O_4@GA@IG. The catalytic activity of Fe_3O_4@GA@IG was investigating in a pseudofour component reaction for the synthesis of polyhydroquinoline and 1,4-DHP derivatives. To obtain the optimal conditions, the reaction between 4-chlorobenzaldehyde (**2b**), ethyl acetoacetate (**3**), dimedone (**4**), and ammonium acetate (**6**) with 1:1:1:1 molar ratios and the reaction between 4-chlorobenzaldehyde (**2b**), dimedone (**4**) or cyclohexanedione (**5**), and ammonium acetate (**6**) with 1:2:1 molar ratios were selected as the model reactions for the synthesis of polyhydroquinoline and 1,4-DHP, respectively.

The effects of various parameters such as the catalyst, solvent, temperature, and energy sources were investigated on the rate and yield of the polyhydroquinoline and 1,4-DHP synthesis reaction (Table 1). As can be seen (Table 1, entry 1−4), in the absence of any catalyst, with or without solvent, at room temperature or at reflux in ethanol, the reaction yield was very low. The effect of ultrasound on the reaction rate is well-evinced, although the reaction time decreases to half, but the yield remains mediocre (entry 5). When Fe_3O_4@GA@IG (5 mg) was used as the catalyst in ethanol at room temperature, the yield increased moderately (entry 6); however, the increase in catalyst loading has not been favorable. Obviously, we studied the synergistic effect of ultrasound and the catalyst, and as expected, the yield has increased remarkably, whereas the reaction time has decreased (entry 9). The reaction was carried out in other solvents, such as water, acetonitrile, and chloroform, but none of these solvents were found to be effective. Finally, to show that the catalytic characteristics of the components of the hybrid material have been improved, Fe_3O_4 and IG were used separately (entries 17, 18). As could be guessed, the use of this hybrid system shows a higher activity

DOI: 10.1021/acsomega.8b00379
ACS Omega 2018, 3, 5012−5020

Table 2. Synthesis of 1,4-DHP and Polyhydroquinoline Derivatives in Ethanol under Ultrasound Irradiation

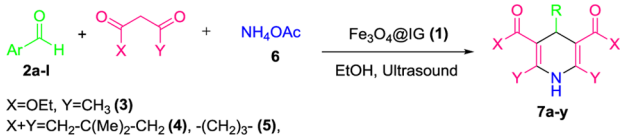

entry	aldehyde	1,3-dicarbonyl	product	time (min)	yield (%)	mp (°C)	lit. mp (°C)
1	benzaldehyde	4	**7a**	50	88	283–286	285–289[15]
2	4-chlorobenzaldehyde	4	**7b**	35	92	295–298	298–299[15]
3	4-fluorobenzaldehyde	4	**7c**	40	90	274–277	274–276[16]
4	2-chlorobenzaldehyde	4	**7d**	40	91	210–214	213[16]
5	2,4-dichlorobenzaldehyde	4	**7e**	35	90	315–318	312[16]
6	3-bromobenzaldehyde	4	**7f**	50	89	295–298	294–297[17]
7	2-nitrobenzaldehyde	4	**7g**	40	90	282–286	284–287[18]
8	4-methylbenzaldehyde	4	**7h**	60	82	268–270	270–275[15]
9	4-methoxybenzaldehyde	4	**7i**	70	80	274–276	275–277[15]
10	3-hydroxybenzaldehyde	4	**7j**	70	77	300–301	302[19]
11	4-hydroxybenzaldehyde	4	**7k**	70	81	270–271	271–274[16]
12	thiophene-2-carbaldehyde	4	**7l**	60	84	309–310	306–308[20]
13	benzaldehyde	5	**7m**	60	75	280	279–281[21]
14	4-chlorobenzaldehyde	5	**7n**	45	89	263–265	266–268[22]
15	4-methoxybenzaldehyde	5	**7o**	70	61	300–301	303–305[21]
16	benzaldehyde	3	**7p**	60	80	158–160	159–160[23]
17	4-chlorobenzaldehyde	3	**7q**	50	90	132–134	136–139[23]
18	2-chlorobenzaldehyde	3	**7r**	55	90	78–80	80–82[23]
19	2,4-dichlorobenzaldehyde	3	**7s**	50	93	150–153	153–155[23]
20	4-methylbenzaldehyde	3	**7t**	60	72	129–130	133–136[23]
21	4-methoxybenzaldehyde	3	**7u**	60	70	154–155	153–155[23]
22	4-hydroxybenzaldehyde	3	**7v**	60	71	230–232	227–229[23]
23	furfural	3	**7w**	50	88	159–160	161[23]
24	thiophene-2-carbaldehyde	3	**7x**	60	80	173–175	170–172[43]
25	cinnamaldehyde	3	**7y**	50	93	144–146	145–147[44]

Table 3. Comparison of the Fe_3O_4@GA@IG Nanocomposite as a Catalyst for the Synthesis of 1,4-DHP and Polyhydroquinoline Derivatives with Other Catalysts and Procedures

entry	cat. & cat. amount	solvent	condition	time	yield (%)	refs
1	$Al_2(SO_4)_3$, 10 mol %	ethanol	reflux	8 h	92	24
2	La_2O_3, 10 mol %	TFE	rt	1–1.5 h	89	25
3	$BiBr_3$, 2 mol %	ethanol	rt	2 h	86	26
4	Fe_3O_4@GA@IG, 10 mg	ethanol	ultrasound	20 min	94	this work

and higher yield in a shorter reaction time. As a result, the optimum condition was the use of 10 mg of Fe_3O_4@GA@IG under ultrasonic irradiation in ethanol as the solvent (entry 15).

To further explore the effectiveness of the Fe_3O_4@GA@IG bionanocatalyst and extend the scope of this protocol, the reaction between various aromatic aldehydes **2a–l**, ammonium acetate (**6**), and 1,3-dicarbonyl compounds **3**, **4**, and **5** under optimized conditions was realized, and the results are shown in Table 2.

The two pathways [A] and [B] of the plausible mechanism consist of a sequence of consecutive reactions proposed in Scheme 2. In path [A], the reaction proceeds through an acid–base bifunctional catalyst. Initially, the acidic sites of the bionanocatalyst activated the aldehyde by protonation; on the other hand, the acidic hydrogen of the 1,3-dicarbonyl compounds was captured by the amine group of the bionanocatalyst; these electrophiles and nucleophiles reacted together and created the Knoevenagel intermediate [**I**] that undergoes a Michael reaction with the second enolizable 1,3-dicarbonyl compound producing the intermediate [**II**]. The Michael product [**II**] reacted with ammonium acetate forming an enamine that endures intramolecular cyclization followed by dehydration, yielding the desired product.

A comparison between this work and previous reported methods for the synthesis of 1,4-DHP and polyhydroquinoline derivatives has been done, and the results are tabulated in Table 3. The capacity and effectiveness of the prepared catalyst, Fe_3O_4@GA@IG, is clearly revealed.

2.3. Synthesis of 2-Amino-4*H*-pyran Derivatives by Fe_3O_4@GA@IG. To reach the optimal conditions, the reaction between 4-chlorobenzaldehyde (**2b**), dimedone (**5**), and malononitrile (**9**) with 1:1:1 molar ratios was selected as the model reaction. The effects of various parameters such as the catalyst, solvent, temperature, and energy sources on the rate and yield of the 2-amino-4*H*-pyran derivatives were investigated for the model reaction (Table 4). As the results indicate, the optimum condition was the use of 20 mg of Fe_3O_4@GA@IG under reflux in ethanol (entry 11).

To expand the scope and practical application of this bionanocatalyst and method, a three-component reaction

DOI: 10.1021/acsomega.8b00379
ACS Omega 2018, 3, 5012–5020

Table 4. Optimization of the Catalyst, Synthesis Condition, and Solvent for the Synthesis of 4*H*-Pyran on the Model Reaction

entry	cat. & cat. amount (mg)	solvent	temp. (°C)	time (min)	yield (%)
1			rt	120	trace
2			80	120	trace
3		ethanol	rt	120	10
4		ethanol	reflux	120	17
5	Fe_3O_4@GA@IG (10)	ethanol	rt	120	25
6	Fe_3O_4@GA@IG (10)	ethanol	50	100	38
7	Fe_3O_4@GA@IG (10)	ethanol	reflux	40	84
8	Fe_3O_4@GA@IG (10)	acetonitrile	reflux	60	52
9	Fe_3O_4@GA@IG (10)	chloroform	reflux	75	50
10	Fe_3O_4@IG (20)	ethanol	ultrasound	60	51
11	Fe_3O_4@IG (20)	**ethanol**	**reflux**	**15**	**92**
12	Fe_3O_4@IG (25)	ethanol	reflux	15	92
13	Fe_3O_4@GA@IG (5)	ethanol	reflux	60	83
14	Fe_3O_4 NPs (20)	ethanol	reflux	60	54
15	IG (20)	ethanol	reflux	50	67

Scheme 3. Plausible Mechanism for the Synthesis of 4*H*-Pyran Derivatives

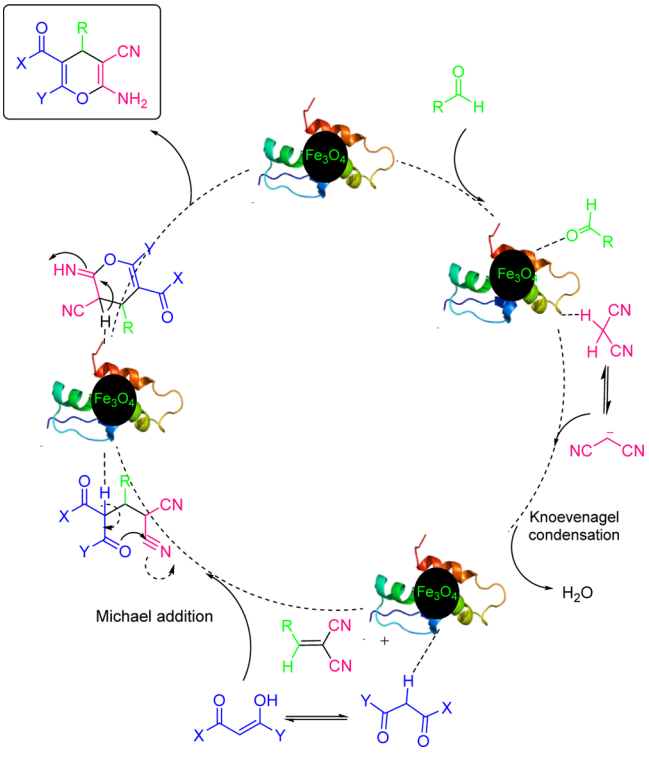

among various aromatic aldehydes (**2a–l**), malononitrile (**9**), and 1,3-dicarbonyl compounds **3**, **4**, **5**, and **8** was investigated under optimal conditions, and the results are demonstrated in Table 5.

The proposed mechanism for the three-component reaction of aldehyde, malononitrile, and 1,3-dicarbonyl compounds in the presence of Fe_3O_4@GA@IG is shown in Scheme 3.

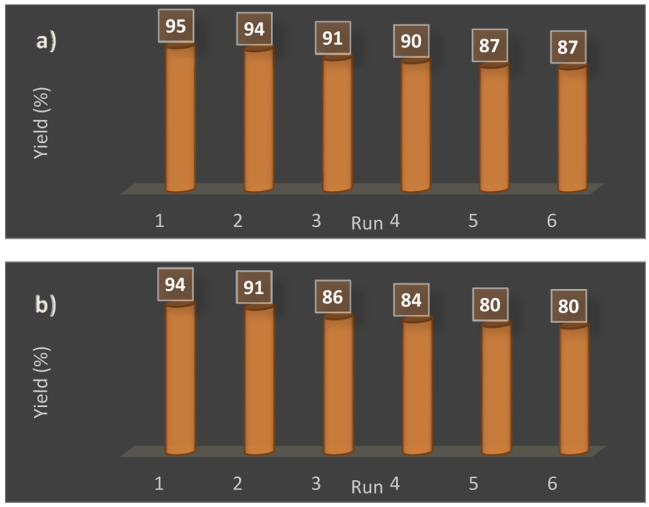

Figure 8. Recyclability of the catalyst for (a) 4*H*-pyran and (b) 1,4-DHP.

A comparison between the previously published works and our method could highlight the capacity and efficiency of the prepared catalyst Fe_3O_4@GA@IG for the synthesis of 4*H*-pyran derivatives (Table 6).

2.4. Investigating the Recyclability of Fe_3O_4@GA@IG in Hantzsch Reaction. One of the advantages of heterogeneous catalysts is the easy separation and recyclability. In this regard, the recyclability and reuse of the magnetic bionanocatalyst was evaluated in the model reaction. At the end of the reaction, Fe_3O_4@GA@IG was collected by an external magnetic field and then washed with ethyl acetate, normal hexane, and ethanol and then dried in an oven at 50 °C. The recycled magnetic nanocatalyst was used for six consecutive times in the model reaction. According to the results illustrated in Figure 8, there is no appreciable reduction in the efficiency of the Fe_3O_4@GA@IG catalyst. FTIR spectra of the recycled catalyst were recorded after six cycles and compared with the fresh catalyst (Figure 1c,d). It can be clearly seen that the used catalyst has not undergone any structural changes.

3. CONCLUSIONS

In summary, a new biocompatible IG-based core/shell MNP, Fe_3O_4@GA@IG, was prepared, characterized, and its catalytic activity was verified. Fe_3O_4@GA@IG was proven to be a bionanocatalyst for the synthesis of 1,4-DHP and 4*H*-pyran derivatives via two one-pot three-component reactions under sonication in ethanol. This method offers several advantages such as the use of ultrasound waves as an alternative green source of energy, omitting toxic solvents or catalysts, good yields, short reaction times, very simple workup, magnetically separable, recyclable, and green catalyst obtained from a natural source. This catalyst showed suitable recyclability with no significant yield decrease after six runs. Given its performance, it can be used in other acid−base-catalyzed reactions.

4. EXPERIMENTAL SECTION

4.1. Materials. All reagents and materials were purchased from commercial sources and used without purification. All of them were analytical grade. The swim bladders were obtained from common carp of Caspian Sea. SEM analysis was performed by using KYKY-EM3200 (26 kV). TEM analysis was carried out by EM10C-100 kV. XRD analysis was done by

DOI: 10.1021/acsomega.8b00379
ACS Omega 2018, 3, 5012−5020

Table 5. One-Pot Synthesis of 4*H*-Pyran Derivatives in Refluxing Ethanol

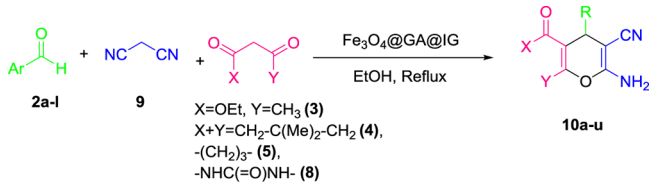

entry	aldehyde	1,3-dicarbonyl	product	time (min)	yield (%)	mp (°C)	lit. mp (°C)
1	4-chlrobenzaldehyde	**3**	**10a**	60	90	172–174	174–175[27]
2	4-nitrobenzaldehyde	**3**	**10b**	60	92	182–186	183–185[27]
3	4-methylbenzaldehyde	**3**	**10c**	95	82	175–177	177–179[27]
4	4-methoxybenzaldehyde	**3**	**10d**	110	78	135–137	136–137[27]
5	3-nitrobenzaldehyde	**3**	**10e**	15	95	199–202	198–200[27]
6	4-chlrobenzaldehyde	**4**	**10f**	15	92	214–216	215–216[28]
7	4-cyanobenzaldehyde	**4**	**10g**	20	90	229–231	228–229[27]
8	3-nitrobenzaldehyde	**4**	**10h**	20	90	216–218	214–216[29]
9	4-methoxybenzaldehyde	**4**	**10i**	50	85	200–203	201–202[27]
10	furfural	**4**	**10j**	90	80	221–224	221–224[30]
11	4-chlrobenzaldehyde	**5**	**10k**	20	91	222–225	223–226[30]
12	4-cyanobenzaldehyde	**5**	**10l**	30	90	237–238	235–237[31]
13	3-nitrobenzaldehyde	**5**	**10m**	35	89	197–200	200–202[20]
14	4-methoxybenzaldehyde	**5**	**10n**	90	83	206–209	207–209[32]
15	furfural	**5**	**10o**	85	81	236–239	237–239[30]
16	thiophene-2-carbaldehyde	**5**	**10p**	40	96	223–224	223–225[42]
17	4-chlrobenzaldehyde	**8**	**10q**	25	90	232–236	234–236[29]
18	2-nitrobenzaldehyde	**8**	**10r**	30	91	257–258	255–257[29]
19	benzaldehyde	**8**	**10s**	40	88	208–210	209–210[34]
20	4-methylbenzaldehyde	**8**	**10t**	50	85	228–230	226–227[34]
21	4-methoxybenzaldehyde	**8**	**10u**	65	89	282–283	280–281[34]

Table 6. Comparison of the Fe_3O_4@GA@IG Nanocomposite as a Catalyst for the Synthesis of 4*H*-Pyran Derivatives with Other Catalysts and Procedures

entry	cat. & cat. amount	solvent	condition	time (min)	yield (%)	reference
1	SiO_2 NPs (5 mg)	EtOH	rt	40	86–94	35
2	SBPPSP (50 mg)	EtOH/H_2O (1:1)	reflux	20	92	36
3	SB-DABCO (6 mol %)	EtOH	rt	35	96	37
4	NH_4OAc (1.5 mol)		rt	15	59–78	45
5	Fe_3O_4@GA@IG (20 mg)	EtOH	reflux	15	92	this work

Holland Philips Xpert, Co K and ultrasonicated by Topsonics, 20 KHz, 400 W. ^1H and ^{13}C NMR spectra were recorded on Bruker AVANCE DPX 500. The chemical shifts (δ) are given in parts per million and referenced to the tetramethylsilane internal standard. IR spectra were recorded in KBr on a Shimadzu FT-IR spectrometer and were reported in wavenumbers (cm^{-1}). All melting points were measured on a capillary melting point apparatus.

4.2. General Procedure for the Preparation of Fe_3O_4 NPs. The MNPs was synthesized using a coprecipitation method described previously.[41] In a typical procedure, $FeCl_3 \cdot 6H_2O$ (5.20 g) and $FeCl_2 \cdot 4H_2O$ (2.00 g) (Fe^{2+}/Fe^{3+} = 2:1) were dissolved in deionized water (25 mL) purged with N_2 to get a homogenous solution. Chemical precipitation was performed by the slow addition of NaOH solution (1.50 mg L^{-1}), under vigorous stirring at 80 °C for 60 min, until the pH = 10 was reached. The precipitate was separated from the solution by an external magnetic field, washed three times with deionized water and ethanol (25 mL), and dried in an oven at 65 °C for 24 h.

4.3. General Procedure for the Preparation of Fe_3O_4@GA@IG. Initially, Fe_3O_4 (0.1 g) and glutaraldehyde (10 mL) were sonicated in ethanol (15 mL) for 15 min. Then, IG (0.1 g) was added to the flask and the mixture was sonicated for 1 h. The prepared magnetite IG was separated by an external magnet and placed in an oven at 60–70 °C for 24 h.

4.4. General Procedure for the Synthesis of 1,4-DHP and Polyhydroquinoline Derivatives. A mixture of aldehyde (1.0 mmol), ammonium acetate (1.0 mmol), 1,3-dicarbonyl (2.0 mmol), and Fe_3O_4@GA@IG (10 mg) in ethanol (2.0 mL) as the solvent was placed into a round-bottom flask and irradiated by an ultrasonic probe sonicator. To synthesize polyhydroquinolin derivatives, aldehyde (1.0 mmol), ammonium acetate (1.0 mmol), dimedone (140.2 mg, 1.0 mmol), 1,3-dicarbonyl (1.0 mmol), and Fe_3O_4@GA@IG (10 mg) in ethanol (2.0 mL) were placed into a round-bottom flask and sonicated. The reaction progression was surveyed by thin-layer chromatography (TLC) using ethyl acetate/hexane (1:3) as the eluent. After completion of the reaction, the catalyst was removed by an external magnet. The pure product was obtained after recrystallization from alcohol–water.

4.5. General Procedure for the Synthesis of 4*H*-Pyran Derivatives. A mixture of aldehyde (1.0 mmol), malononitrile (66 mg, 1.0 mmol), 1,3-dicarbonyl (1.0 mmol), and Fe_3O_4@

DOI: 10.1021/acsomega.8b00379
ACS Omega 2018, 3, 5012–5020

GA@IG (20 mg) in ethanol (3 mL) was stirred at the reflux condition. The reaction progress was checked by means of TLC technique using ethyl acetate/normal hexane (1:3) as the eluent. After completion of the reaction, the catalyst was removed by an external magnet and the product was crystalized and separated from the residual solution by cooling.

■ ASSOCIATED CONTENT

Supporting Information

The Supporting Information is available free of charge on the ACS Publications website at DOI: 10.1021/acsomega.8b00379.

^{1}H NMR spectra of compounds (7b, 7k, 7l, 7x, and 7y) and (10e, 10f, and 10i) (PDF)

■ AUTHOR INFORMATION

Corresponding Author

*E-mail: shjavan@iust.ac.ir (S.J.).

ORCID

Shahrzad Javanshir: 0000-0002-3161-0456

Ali Maleki: 0000-0001-5490-3350

Author Contributions

The manuscript was written through contributions of all authors. All authors have given approval to the final version of the manuscript.

Notes

The authors declare no competing financial interest.

■ ACKNOWLEDGMENTS

The authors wish to express their gratitude for the financial support provided by the Research Council of Iran University of Science and Technology (IUST), Tehran, Iran.

■ REFERENCES

(1) Mason, T. J.; Lorimer, J. P. *Applied Sonochemistry: The Uses of Power Ultrasound in Chemistry and Processing*; Wiley-VCH, 2002; Vol. *0*.

(2) Xu, H.; Zeiger, B. W.; Suslick, K. S. Sonochemical Synthesis of Nanomaterials. *Chem. Soc. Rev.* **2013**, *42*, 2555−2567.

(3) Caruso, F. Nanoengineering of Particle Surfaces. *Adv. Mater.* **2001**, *13*, 11−22.

(4) Feng, X.; Mao, C.; Yang, G.; Hou, W.; Zhu, J.-J. Polyaniline/Au Composite Hollow Spheres: Synthesis, Characterization, and Application to the Detection of Dopamine. *Langmuir* **2006**, *22*, 4384−4389.

(5) Salgueiriño-Maceira, V.; Correa-Duarte, M. A.; Spasova, M.; Liz-Marzán, L. M.; Farle, M. Composite Silica Spheres with Magnetic and Luminescent Functionalities. *Adv. Funct. Mater.* **2006**, *16*, 509−514.

(6) Polshettiwar, V.; Luque, R.; Fihri, A.; Zhu, H.; Bouhrara, M.; Basset, J.-M. Magnetically Recoverable Nanocatalysts. *Chem. Rev.* **2011**, *111*, 3036−3075.

(7) Hickman, D.; Sims, T. J.; Miles, C. A.; Bailey, A. J.; de Mari, M.; Koopmans, M. Isinglass/collagen: Denaturation and Functionality. *J. Biotechnol.* **2000**, *79*, 245−257.

(8) Leach, A. A.; Barrett, J. Collagen Chemistry in Relation To Isinglass and Isinglass Finings. Part II. *J. Inst. Brew.* **1967**, *73*, 376−381.

(9) Javanshir, S.; Pourshiri, N. S.; Dolatkhah, Z.; Farhadnia, M. Caspian Isinglass, a Versatile and Sustainable Biocatalyst for Domino Synthesis of Spirooxindoles and Spiroacenaphthylenes in Water. *Monatsh. Chem.* **2017**, *148*, 703−710.

(10) Hemmati, B.; Javanshir, S.; Dolatkhah, Z. Hybrid Magnetic Irish moss/Fe_3O_4 as a Nano-Biocatalyst for Synthesis of Imidazopyrimidine Derivatives. *RSC Adv.* **2016**, *6*, 50431−50436.

(11) Brahmachari, G. *Green Synthetic Approaches for Biologically Relevant Heterocycles*; Brahmachari, G., Ed.; Elsevier Science & Technology Books: Santiniketan, 2015.

(12) Sharma, V. K.; Singh, S. K. Synthesis, Utility and Medicinal Importance of 1,2- & 1,4-Dihydropyridines. *RSC Adv.* **2017**, *7*, 2682−2732.

(13) Azzam, R. A.; Mohareb, R. M. Multicomponent Reactions of Acetoacetanilide Derivatives with Aromatic Aldehydes and Cyano-methylene Reagents to Produce 4H-Pyran and 1,4-Dihydropyridine Derivatives with Antitumor Activities. *Chem. Pharm. Bull.* **2015**, *63*, 1055−1064.

(14) Ruiz, E.; Rodríguez, H.; Coro, J.; Niebla, V.; Rodríguez, A.; Martínez-Alvarez, R.; de Armas, H. N.; Suárez, M.; Martín, N. Efficient Sonochemical Synthesis of Alkyl 4-Aryl-6-Chloro-5-Formyl-2-Methyl-1,4-Dihydropyridine-3-Carboxylate Derivatives. *Ultrason. Sonochem.* **2012**, *19*, 221−226.

(15) Abdollahi-Alibeik, M.; Rezaeipoor-Anari, A. Fe_3O_4@B-MCM-41: A New Magnetically Recoverable Nanostructured Catalyst for the Synthesis of Polyhydroquinolines. *J. Magn. Magn. Mater.* **2016**, *398*, 205−214.

(16) Khaligh, N. G. Four-component one-pot synthesis of unsymmetrical polyhydroquinoline derivatives using 3-methyl-1-sulfonic acid imidazolium hydrogen sulfate as a catalyst. *Chin. J. Catal.* **2014**, *35*, 1036−1042.

(17) Li, B. L.; Zhong, A. G.; Ying, A. G. Novel SO3H-Functionalized Ionic Liquids − Catalyzed Facile and Efficient Synthesis of Polyhydroquinoline Derivatives via Hantzsch Condensation under Ultrasound Irradiation. *J. Heterocycl. Chem.* **2014**, *52*, 445−449.

(18) Zarnegar, Z.; Safari, J.; Kafroudi, Z. M. Co_3O_4−CNT Nanocomposites: A Powerful, Reusable, and Stable Catalyst for Sonochemical Synthesis of Polyhydroquinolines. *New J. Chem.* **2015**, *39*, 1445−1451.

(19) Ghorbani-Choghamarani, A.; Azadi, G. Synthesis, Characterization, and Application of Fe_3O_4-SA-PPCA as a Novel Nanomagnetic Reusable Catalyst for the Efficient Synthesis of 2,3-Dihydroquinazolin-4(1H)-Ones and Polyhydroquinolines. *RSC Adv.* **2015**, *5*, 9752−9758.

(20) Nasr-Esfahani, M.; Elhamifar, D.; Amadeh, T.; Karimi, B. Periodic Mesoporous Organosilica with Ionic-Liquid Framework Supported Manganese: An Efficient and Recyclable Nanocatalyst for the Unsymmetric Hantzsch Reaction. *RSC Adv.* **2015**, *5*, 13087−13094.

(21) Vahdat, S. M.; Khaksar, S.; Baghery, S. An Efficient One-Pot Synthesis of Bis(Indolyl)Methanes Catalyzed by Ionic Liquid with Multi-SO3H Groups under Ambient Temperature in Water. *World Appl. Sci. J.* **2011**, *15*, 877−884.

(22) Maleki, B.; Tayebee, R.; Sepehr, Z.; Kermanian, M. A Novel, Hetero Geneous and Recyclable Polymeric Catalyst for the One-Pot Synthesis of Polyhydroquinoline and 1,8-Dioxohexahydroacridine Derivatives Under Solvent-Free Conditions. *Acta Chim. Slov.* **2012**, *59*, 814−823.

(23) Kidwai, M.; Bhatnagar, D. Polyethylene Glycol-Mediated Synthesis of Decahydroacridine-1,8-Diones Catalyzed by Ceric Ammonium Nitrate. *Chem. Pap.* **2010**, *64*, 825−828.

(24) Kulkarni, P. $Al_2(SO_4)_3$ is an efficient and mild acid catalyst for the one-pot, four-component synthesis of polyhydroquinoline. *J. Chil. Chem. Soc.* **2014**, *59*, 2319−2321.

(25) Tekale, S. U.; Pagore, V. P.; Kauthale, S. S.; Pawar, R. P. La2O3/TFE: An Efficient System for Room Temperature Synthesis of Hantzsch Polyhydroquinolines. *Chin. Chem. Lett.* **2014**, *25*, 1149−1152.

(26) Yoo, J. S.; Laughlin, T. J.; Krob, J. J.; Mohan, R. S. Bismuth(III) Bromide Catalyzed Synthesis of Polyhydroquinoline Derivatives via the Hantzsch Reaction. *Tetrahedron Lett.* **2015**, *56*, 4060−4062.

(27) Amirnejad, M.; Naimi-Jamal, M. R.; Tourani, H.; Ghafuri, H. A Facile Solvent-Free One-Pot Three-Component Method for the Synthesis of 2-Amino-4H-Pyrans and Tetrahydro-4H-Chromenes at Ambient Temperature. *Monatsh. Chem.* **2013**, *144*, 1219−1225.

(28) Dekamin, M. G.; Ilkhanizadeh, S.; Latifidoost, Z.; Daemi, H.; Karimi, Z.; Barikani, M. Alginic Acid: A Highly Efficient Renewable

DOI: 10.1021/acsomega.8b00379
ACS Omega 2018, 3, 5012−5020

and Heterogeneous Biopolymeric Catalyst for One-Pot Synthesis of the Hantzsch 1,4-Dihydropyridines. *RSC Adv.* **2014**, *4*, 56658.
(29) Mashkouri, S.; Naimi-Jamal, M. R. Mechanochemical Solvent-Free and Catalyst-Free One-Pot Synthesis of pyrano[2,3-D]-pyrimidine-2,4(1H,3H)-Diones with Quantitative Yields. *Molecules* **2009**, *14*, 474−479.
(30) Sabitha, G.; Arundhathi, K.; Sudhakar, K.; Sastry, B. S.; Yadav, J. S. Cerium(III) Chloride−Catalyzed One-Pot Synthesis of Tetrahydrobenzo[B]Pyrans. *Synth. Commun.* **2009**, *39*, 433−442.
(31) Shirini, F.; Abedini, M.; Zarrabzadeh, S.; Seddighi, M. Efficient Synthesis of 4H-Pyran Derivatives Using a Polymeric Catalyst Based on PVP. *J. Iran. Chem. Soc.* **2015**, *12*, 2105−2113.
(32) Rostamnia, S.; Nuri, A.; Xin, H.; Pourjavadi, A.; Hosseini, S. H. Water Dispersed Magnetic Nanoparticles (H2O-DMNPs) of γ-Fe2O3for Multicomponent Coupling Reactions: A Green, Single-Pot Technique for the Synthesis of Tetrahydro-4H-Chromenes and Hexahydroquinoline Carboxylates. *Tetrahedron Lett.* **2013**, *54*, 3344−3347.
(33) Shestopalov, A. A.; Rodinovskaya, L. A.; Shestopalov, A. M.; Litvinov, V. P. Single-Step Synthesis of Substituted 7-aminopyrano-[2,3-D]pyrimidines. *Russ. Chem. Bull.* **2004**, *53*, 2342.
(34) Gao, Y.; Tu, S.; Li, T.; Zhang, X.; Zhu, S.; Fang, F.; Shi, D. Effective Synthesis of 7-Amino-6-cyano-5-aryl-5H-pyrano[2,3-D]-pyrimidine-2,4(1H,3H)-diones Under Microwave Irradiation. *Synth. Commun.* **2004**, *34*, 1295−1299.
(35) Banerjee, S.; Horn, A.; Khatri, H.; Sereda, G. A Green One-Pot Multicomponent Synthesis of 4H-Pyrans and Polysubstituted Aniline Derivatives of Biological, Pharmacological, and Optical Applications Using Silica Nanoparticles as Reusable Catalyst. *Tetrahedron Lett.* **2011**, *52*, 1878−1881.
(36) Niknam, K.; Borazjani, N.; Rashidian, R.; Jamali, A. Silica-Bonded N-Propylpiperazine Sodium N-Propionate as Recyclable Catalyst for Synthesis of 4H-Pyran Derivatives. *Chin. J. Catal.* **2013**, *34*, 2245.
(37) Hasaninejad, A.; Shekouhy, M.; Golzar, N.; Zare, A.; Doroodmand, M. M. Silica Bonded N-Propyl-4-Aza-1-azoniabicyclo[2.2.2]octane Chloride (SB-DABCO): A Highly Efficient, Reusable and New Heterogeneous Catalyst for the Synthesis of 4H-Benzo[b]pyran Derivatives. *Appl. Catal., A* **2011**, *402*, 11−22.
(38) Bodaghifard, M. A.; Mobinikhaledi, A.; Asadbegi, S. Bis(4-Pyridylamino)triazine-Stabilized Magnetite Nanoparticles: Preparation, Characterization and Application as a Retrievable Catalyst for the Green Synthesis of 4 H -Pyran, 4 H -Thiopyran and 1,4-Dihydropyridine Derivatives. *Appl. Organomet. Chem.* **2017**, *31*, No. e3557.
(39) Abaszadeh, M.; Seifi, M. Crown Ether Complex Cation Ionic Liquids: Synthesis and Catalytic Applications for the Synthesis of Tetrahydro-4 H -Chromene and 1,4-Dihydropyridine Derivatives. *J. Sulfur Chem.* **2017**, *38*, 440−449.
(40) Maddila, S.; Gangu, K. K.; Maddila, S. N.; Jonnalagadda, S. B. A Facile, Efficient, and Sustainable chitosan/CaHAp Catalyst and One-Pot Synthesis of Novel 2,6-Diamino-Pyran-3,5-Dicarbonitriles. *Mol. Diversity* **2017**, *21*, 247−255.
(41) Wu, S.; Sun, A.; Zhai, F.; Wang, J.; Xu, W.; Zhang, Q.; Volinsky, A. A. Fe_3O_4 magnetic Nanoparticles Synthesis from Tailings by Ultrasonic Chemical Co-Precipitation. *Mater. Lett.* **2011**, *65*, 1882−1884.
(42) Peng, H. N.; Zheng, D. G.; Peng, X. M. p-Toluene sulfonic acid catalyzed one-pot synthesis of unsymmetrical 1,4-dihydropyridines derivatives via Hantzsch reaction. *Asian J. Chem.* **2011**, *23*, 1833−1837.
(43) Safaei-Ghomi, J.; Ziarati, A.; Zahedi, S. Silica (NPs) supported Fe (III) as a reusable heterogeneous catalyst for the one-pot synthesis of 1, 4-dihydropyridines under mild conditions. *J. Chem. Sci.* **2012**, *124*, 933−939.
(44) Wang, X.; Gong, H.; Quan, Z.; Li, L.; Ye, H. One-Pot, Three-Component Synthesis of 1,4-Dihydropyridines in PEG-400. *Synth. Commun.* **2011**, *41*, 3251−3258.
(45) Smits, R.; Belyakov, S.; Plotniece, A.; Duburs, G. Synthesis of 4H-Pyran Derivatives Under Solvent-Free and Grinding Conditions. *Synth. Commun.* **2013**, *43*, 465−475.

DOI: 10.1021/acsomega.8b00379
ACS Omega 2018, 3, 5012−5020